Bull. Mar. Sci & Tech 11(1), 2002
Research Institute of Marine Science and Technology
Korea Maritime University

Null-broadening in a waveguide

J. S. Kim,[a] W. S. Hodgkiss, W. A. Kuperman, and H. C. Song
Marine Physical Laboratory/Scripps Institution of Oceanography, University of California, San Diego, La Jolla, California 92093-0238

(Received 1 March 2001; revised 25 March 2002; accepted 20 April 2002)

Null-broadening, introduced in plane wave beamforming, is extended to an ocean waveguide in the context of matched field processing. The method is based on the minimum variance processor with white noise constraint and the distribution of fictitious sources using the theory of waveguide invariants. The proposed method is demonstrated in simulation as well as with data collected during the SWellEx-96 experiment. As another application, it is shown that the width of a null can be controlled in an adaptive time reversal mirror with a source-receive array. © *2002 Acoustical Society of America.* [DOI: 10.1121/1.1488139]

PACS numbers: 43 60.Gk, 43.30.Wi, 43.20.Fn [SAC]

I. INTRODUCTION

Controlling the shape of a spatial filter is a useful technique in transmission and reception with an adaptive array. The adaptive beam pattern is generated via adaptive weights on the array, for example, to broaden the main lobe or a null as well as to reduce the sidelobes of the spatial filter. Recently, null-broadening in plane wave beamforming (PBF) has been introduced by Mailloux[1] and Zatman[2] and Guerci[3] derived a covariance matrix taper (CMT) function to broaden a null. In the current paper, null-broadening is extended to a waveguide utilizing the theory of waveguide invariants.

Null-broadening provides robust adaptive nulling in passive array signal processing when the sources of interference are confined to either a specific direction (plane wave beamforming) or a specific cell (matched field processing). Moreover, in the transmission of acoustic energy, the null-broadening technique provides robust null-steering and control of the null-width in a temporally fluctuating ocean environment. Therefore, the objective of this paper is to develop a method to broaden nulls in an ocean waveguide in the context of matched field processing (MFP).

In order to broaden a null in a waveguide, the theory of waveguide invariants[4–7] is utilized to augment the fictitious interferers in the vicinity of a true interferer. When the minimum variance processor with white noise constraint is applied to minimize the power coming from other than the look-direction, nulls are placed in the fictitious interferer locations so as to broaden the null. The method is applied here to the ocean waveguide to demonstrate null-broadening in simulation and with ocean data. As another application, the method is employed to broaden the null steered by an adaptive time reversal mirror.[8]

In Sec. II, the null-broadening method in plane wave beamforming is reviewed and the implication of using short-length fast Fourier transforms (FFT's) to find adaptive weights is discussed. The null-broadening method in a waveguide is developed and realized via simulation in Sec. III. In Sec. IV, ocean acoustic data is analyzed to show the effect of null-broadening in matched field processing. As another application, null-broadening with an adaptive time reversal mirror (ATRM) is demonstrated in Sec. V.

II. NULL-BROADENING IN PLANE WAVE BEAMFORMING: FREE SPACE

In plane wave beamforming, a technique to make a null broader by tapering the cross-spectral density matrix (CSDM) has been developed by augmenting the CSDM with multiple interferers in the vicinity of the true interferer location[1] and by dispersion synthesis.[2] These two approaches use different formulations but are based on the same principle of distributing the additional interferers around the true location of the interferer.

The plane wave beamforming derivations which are simple and instrumental in extending their approach to matched field processing (MFP) in an ocean waveguide are review in Sec. II A. The simulation results are presented in Sec. II B.

A. Theory

In plane wave beamforming, the beam pattern of the Bartlett processor is a correlation between a data vector $\mathbf{d}(\theta_s)$ and the search vector (or steering or replica vector) $\mathbf{d}(\theta)$ which is expressed as

$$B_{BT}(\theta)=\mathbf{d}(\theta_s)^{\dagger}\mathbf{d}(\theta), \tag{1}$$

where θ_s is source direction and $(\ )^{\dagger}$ denotes the Hermitian or conjugate transpose. For the minimum variance distortionless response (MVDR) processor, the weight vector $\mathbf{w}(\theta)$ in the direction θ is

$$\mathbf{w}(\theta)=\frac{\mathbf{K}^{-1}\mathbf{d}(\theta)}{\mathbf{d}^{\dagger}(\theta)\mathbf{K}^{-1}\mathbf{d}(\theta)}, \tag{2}$$

where $\mathbf{K}$ is the cross-spectral density matrix (CSDM) defined as $\mathbf{K}=\Sigma_{\text{source}}\mathbf{d}(\theta_s)\mathbf{d}^{\dagger}(\theta_s)$ assuming the sources are uncorrelated for the moment and ignoring any diffuse or uncorrelated noise at the array. The beam pattern of the MVDR processor while looking at θ_l is

$$B_{\text{MVDR}}(\theta)=\mathbf{w}^{\dagger}(\theta_l)\mathbf{d}(\theta). \tag{3}$$

[a]The work was done during the author's sabbatical leave at MPL. Permanent affiliation: Korea Maritime University, Pu-san 606-791, Korea

The distortionless response in the look-direction requires that

$$B_{\mathrm{MVDR}}(\theta_l)=\mathbf{w}^{\dagger}(\theta_l)\mathbf{d}(\theta_l)=1. \tag{4}$$

The CSDM for plane waves coming from $u_l=\sin\theta_l$, where θ_l is measured from the array normal, can be written as

$$k_{mn}=\sigma_l^2 e^{-i(2\pi/\lambda)(x_m-x_n)u_l}, \tag{5}$$

where σ^2 is the source strength, x_m and x_n represent the location of the mth and nth array elements, $\lambda=c/f$ denotes the wavelength, c is the speed of propagation, and f is frequency.

In order to obtain multiple nulls centered around the direction u_l, Mailloux[1] distributed plane waves coming from N directions as

$$u=u_l+q\delta, \quad \text{for } -\frac{N-1}{2}\leq q\leq\frac{N-1}{2}, \tag{6}$$

where δ is defined as $\delta=W/(N-1)$ to obtain a trough width of W between the outermost nulls. The summation over q can be written as

$$K_{mn}=\sum_q k_{mn}=\sum_q \sigma_l^2 e^{i(2\pi/\lambda)(x_m-x_n)(u_l+q\delta)}$$

$$=\frac{\sin(N\Delta)}{\sin(\Delta)}k_{mn}, \tag{7}$$

where $\Delta=\pi(x_m-x_n)\delta/\lambda$.

Zatman[2] distributed the fictitious sources in a different way. By slightly changing the frequency and keeping the incident direction the same, the array sees the data vector as one coming from a different direction. Thus, the augmentation of the fictitious sources can be achieved by integrating the CSDM over a desired frequency bandwidth

$$K_{mn}=\frac{1}{b_w}\int_{f-b_w/2}^{f+b_w/2}k_{mn}\,df=\frac{\sin(\pi b_w\tau_{mn})}{\pi b_w\tau_{mn}}k_{mn}, \tag{8}$$

where $\tau_{mn}=(x_m-x_n)u_l/c$ is the time delay between elements. Note that Mailloux's formulation directly places the fictitious sources in angular space, while Zatman's formulation uses a frequency perturbed CSDM.

The null-broadening approach can be implemented through the concept of a covariance matrix taper (CMT) where the CSDM is modified by a Hadamard or Schur product tapering function.[3] This is applicable to null-broadening in plane wave beamforming. However, in matched field processing the tapering function is coupled with the individual terms of the mode function so that the tapering function cannot be separated from the CSDM. Fortunately, there exists an invariant property associated with the waveguide that allows us to displace nulls by slightly changing the frequency, thus augmenting the nulls around the true location of the interferer that is to be nulled (the details are discussed in Sec. III A).

B. Plane wave beamforming simulation

The elements of the ideal CSDM with uncorrelated noise can be written[9] as

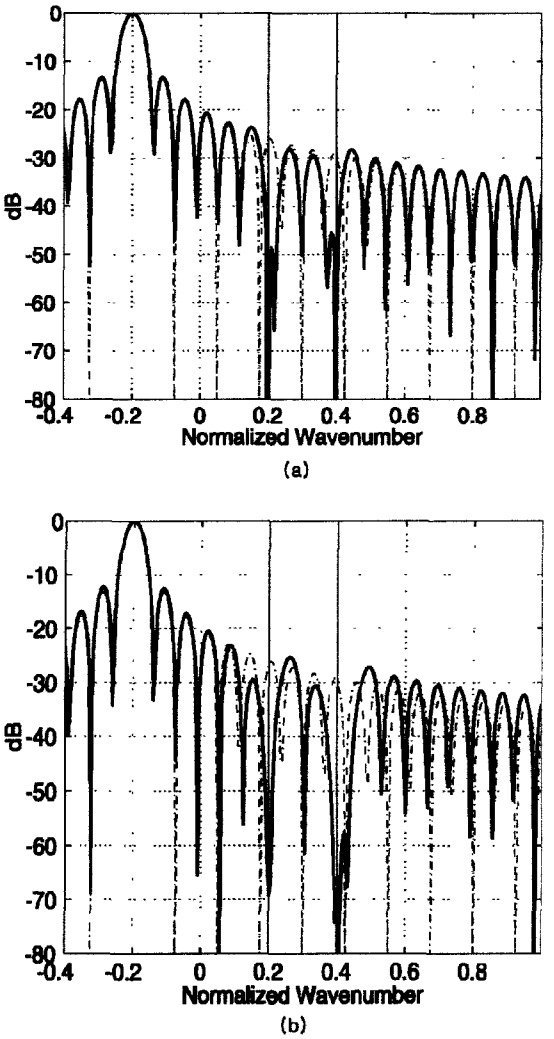

FIG. 1. Beam pattern of the WNC processor for PBF (a) without null-broadening and (b) with null-broadening. The broken line is the beam pattern for a Bartlett processor.

$$k_{mn}=\sum_{l=1}^{3}\sigma_l^2 e^{-i(2\pi\Delta u_l/\lambda)(m-n)}-\sigma_w^2\delta_{mn}. \tag{9}$$

For simulation, one source with $\sigma_1^2=6$ dB, $u_1=-0.2$ and two interferers with $\sigma_2^2=36$ dB, $u_2=0.2$ and $\sigma_3^2=36$ dB, $u_3=0.4$ are used, where u is defined as $u=\sin\theta$. The uncorrelated noise level is $\sigma_w^2=0$ dB. The total number of array elements is $N=64$ and the elements are separated by $\lambda/4$, where λ is the wavelength.

In Fig. 1(a), the beam pattern is shown for the exact CSDM in Eq. (9) while looking at the target at the normalized wave number $u_1=\sin\theta_1=-0.2$. The broken line is the beam pattern of the Bartlett processor and the solid line is that of the MVDR processor with white noise gain constraint (WNC).[10-12] Throughout the paper, -6 dB constraint is used for the WNC processor. The two vertical lines denote the direction of interferers at $u_2=\sin\theta_2=0.2$, and at $u_2=\sin\theta_2=0.4$. It is noted that the WNC beam pattern exhibits nulls in the direction of the interferers. The beam pattern shown in Fig. 1(b) was obtained using the integrated CSDM defined in

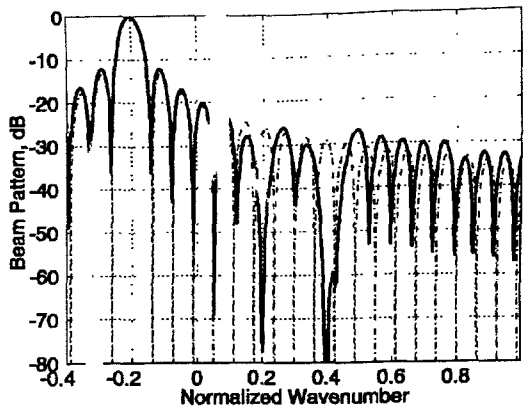

FIG. 2. Beam pa ern with 256 point FFTs and 256 snapshots. The null-broadening is ach ved by using short-length FFTs. The broken line is the beam pattern for a Bartlett processor.

Eq. (8) where $f=100$ Hz and $b_w=5$ Hz. In this case, these results were computed using a 4096-point FFT on independently generated frequency components with frequency resolution of $\Delta f=1/(4096\Delta t)$. Since the sampling rate was 1500 samples/second, $\Delta f=0.3662$ Hz. When the frequency is perturbed, the position of the null seen from the array is calculated from the relation

$$\frac{2\pi}{\lambda}u=\text{const.} \tag{10}$$

which leads to

$$u'=\frac{f}{f'}u \quad \text{or} \quad \frac{\sin\theta'}{\lambda'}=\frac{\sin\theta}{\lambda}, \tag{11}$$

where λ' is the wavelength of the perturbed frequency and, u' is the corresponding null location. It is shown in Fig. 1(a) that the null of the beam pattern is broadened through the use of wideband CSDM. In addition, it is noted that null-broadening is more significant for the source at a larger angle since the width of angular augmentation becomes larger for a larger arrival angle, for a given frequency bandwidth.

C. Effect of using short-length FFTs

When the number of snapshots is limited due to observing a fast moving source, a short-length FFT can be used to increase the number of snapshots involved in estimating the CSDM. In this section, it is shown that the use of a short-length FFT produces the same effect as using the CSDM integrated over frequency and results in null-broadening.

Figure 2 shows the beam pattern obtained using 256 snapshots with 256 point FFTs. The frequency resolution is now $\Delta f=1/(256\Delta t)=5.869$ Hz so that a single FFT bin is as wide as the averaging bandwidth represented in Fig. 1(b). In this case, the CSDM components for the source and two interferers were estimated by averaging outer products of broadband array signal vectors (snapshots). These three components plus uncorrelated noise then were added together to form the CSDM estimate.

III. NULL-BROADENING IN MATCHED FIELD PROCESSING: OCEAN WAVEGUIDE

In this section, a null-broadening algorithm in an ocean waveguide is described in the context of matched field processing.

A beam pattern in plane wave beamforming (PBF) can be viewed as a correlation between a signal vector coming from the look-direction and a family of array steering vectors. When this concept is applied to matched field processing (MFP), the equivalent beam pattern is defined as a correlation between a signal vector coming from the look location and a family of array replica vectors. Thus the MFP replica vectors are a generalized form of the steering vectors in PBF.

In Sec. III A, the null-broadening algorithm is described and then simulation results are shown in Sec. III B.

A. Theory

Unlike null-broadening in plane wave beamforming, the covariance matrix taper (CMT) is not explicitly available for null-broadening of matched field processing in a waveguide. From the perspective of mode theory, this can be attributed to the fact that source depth and range are coupled to the mode sum involving a wavenumber spectrum. However, the theory of waveguide invariants[4-7] can be utilized to derive the signal vectors from adjacent ranges at the same depth when the signal vector at the probe source or the interferer location is known. Thus, the distribution of the interferer around the true interferer location can be achieved. The adaptive minimum variance processor with a white noise constraint will then place nulls around the location of the true interferer and broaden the null.

From the theory of waveguide invariants, signal vectors in the vicinity of the interferer and at the same depth are simply a frequency-shifted signal vector coming from the interferer location. Here, we briefly state the practical form of the theory of waveguide invariants applicable to null-broadening in a waveguide.

In a dispersive and multi-modal waveguide, the lines of constant intensity lead to a constant slope between the certain parameters of the waveguide. The invariant, denoted as β, characterizes the relation between the range r and angular frequency ω as

$$\beta=\frac{r}{\omega}\frac{\delta\omega}{\delta r}. \tag{12}$$

The parameter β defined in Eq. (12) is known to be approximately invariant with respect to range and is equal to one in a Pekeris waveguide. For a Pekeris waveguide, Eq. (12) can be rewritten to calculate the new range r' in terms of new frequency ω':

$$r'=\frac{\omega'}{\omega}r. \tag{13}$$

Equation (13) states that the acoustic field at (r,ω') approximates the value at (r',ω). Therefore, broadband data received at an array can be used to estimate the CSDM in the vicinity of the source range at the same depth so as to place

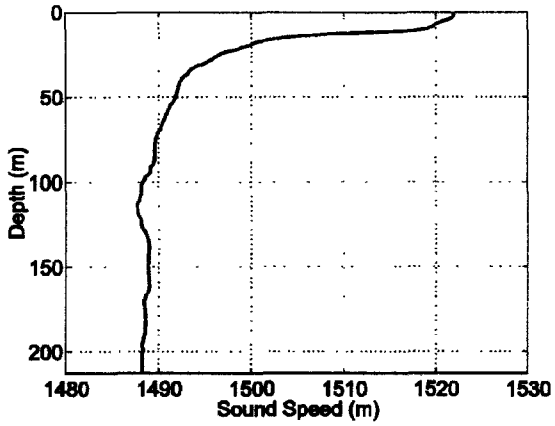

FIG. 3. Sound speed profile for simulation and SWellEx-96 experiment.

a null without measuring the Green's function from fictitious null positions.

B. Simulation with SWellEx-96 environment

The sound profile as a function of depth for our simulation is shown in Fig. 3 which is the same environment as SWellEx-96 experiment.[13] The trajectories of target and interferer assume the same situation as the experiment for the purpose of comparison (see Sec. IV B). The target is at a depth of 20 m and at a range of 5040 m, while the interferer to be nulled is at the same depth and at a range of 3310 m. The radiated power from the interferer is assumed to be 6 dB higher than the radiation from the target.

Since the applicability of the null-broadening technique is dependent on the validity of waveguide invariant theory and the width of the null is determined from the value of β, the transmission loss versus frequency is plotted in Fig. 4. This figure shows that β in Eq. (12) is approximately one as in a Pekeris waveguide.

The simulation results with the ideal CSDM in Fig. 5 display the null-broadening effect at 62 Hz that is to be compared later with the beam pattern from SWellEx-96 data in Fig. 10. Figure 5(a) is for a Pekeris waveguide with the same depth as in SWellEx-96. The broken line is the beam pattern for the conventional matched field processor, the solid line is the beam pattern for the minimum variance processor with white noise constraint (WNC), and the thick solid line is for the same processor as the solid line with null-broadening. In the simulation, since the same sampling parameters are used as in the data analysis, the frequency resolution is given as $\Delta f = 1/(\Delta t * 4096) = 0.3662$ Hz, where $\Delta t = 1/1500$. From Eq. (13), the range shift in a range-independent environment caused by a 7-bin frequency shift is related by the following equation

$$r' = \frac{\omega'}{\omega} r = \frac{2\pi(62 \pm 0.3662 \times 7)}{2\pi \times 62} 3310 = 3310 \pm 140 \text{ m}.$$

The predicted null locations corresponding to the augmented interferers agree well with the null locations shown in Fig. 5(a).

Figure 5(b) shows the nulling pattern as a function of range at a depth of 20 m for the SwellEx-96 experiment. As

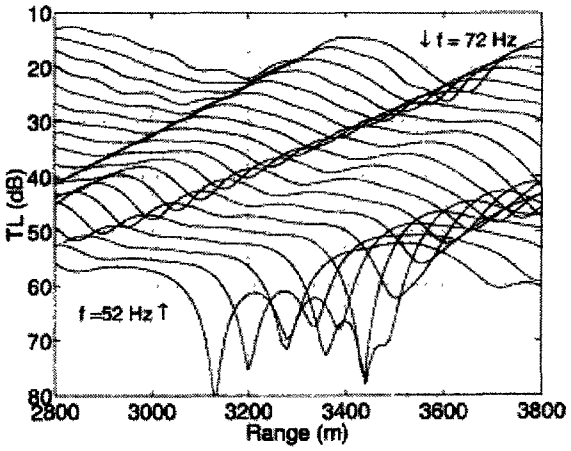

(a)

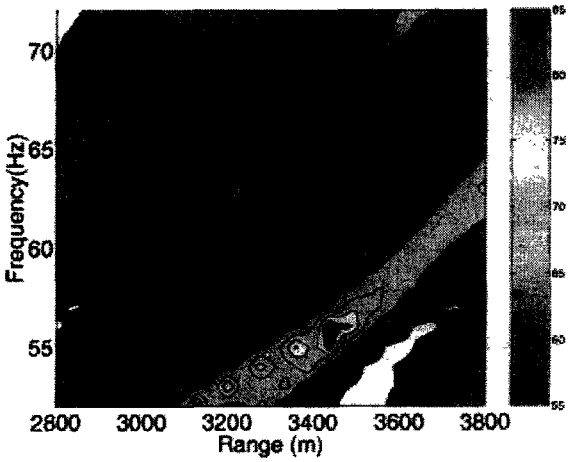

FIG. 4. Waveguide invariant in SWellEx-96. (a) Transmission loss plot (dB) for 52–72 Hz with a 1-Hz interval. (b) Contour plot of (a).

in Fig. 5(a), the broken line is the beam pattern of the Bartlett processor, the solid line represents the beam pattern of WNC without null-broadening, and the thick solid line is WNC with null-broadening. The figure shows that the Bartlett processor is not aware of the interferer, and the null is independent of the location of interferer. However, the beam pattern of WNC places a null at the interferer location $r = 3310$ m.

IV. DEMONSTRATION OF NULL-BROADENING USING OCEAN DATA

In this section, the null-broadening technique is applied to SWellEx-96 data to verify the applicability of the technique to matched field processing in a shallow water waveguide.

In order to apply the null-broadening technique developed in Sec. III, the proper data set requires a wideband signal radiated from a target and an interferer. During the SWellEx-96 experiment, broadband noise radiated from a cargo ship passing by the vertical line array was observed.

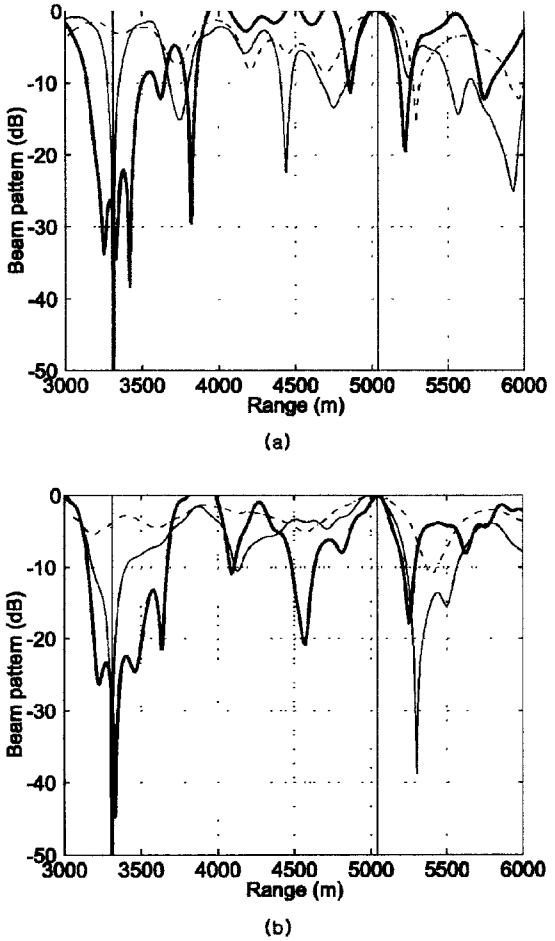

FIG. 5. Simulation with ideal CSDM in (a) Pekeris waveguide and (b) SWellEx-96 environment. The beam pattern of the Bartlett processor is denoted by a broken line, the thin solid line is for WNC without null-broadening, and the thick solid line is for WNC with null-broadening.

Since this data set contains only one broadband noise source as a target, noise from an interferer is simulated by using the data observed at a different time.

In Sec. IV A, the ocean environment and a plan view of the target and interferer are illustrated. The results of null-broadening then are presented in Sec. IV B.

A. Description of SWellEx-96 experiment

The detailed experiment description can be found in Ref. 13. Figure 6(a) shows a plan view of the SwellEx-96 experiment with towed source ship and Fig. 6(b) shows the track of the towed source and interferer. Since the towed source radiates tonals, we are only interested in the broadband noise radiated from the cargo ship. The square marks on the composite radar image shows the track of the cargo ship every 5 min.

B. Two broadband random radiators

In order to apply the null-broadening technique, the following ten frequencies with relatively good signal to noise ratio were used: 53, 54, 56, 59, 60, 62, 66, 69, 72, and 74 Hz. The actual target observed in the data moves from a range of

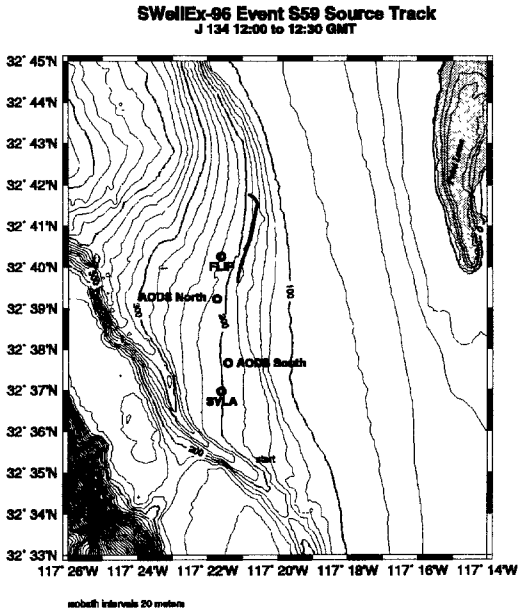

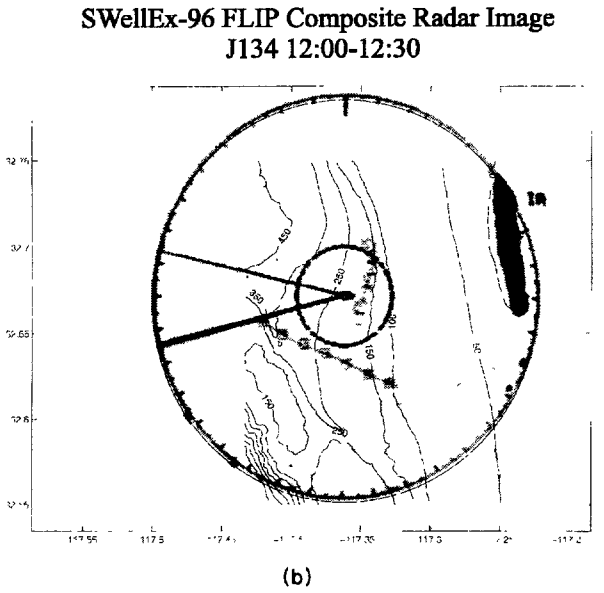

FIG. 6. (a) Plan view of the SWellEx-96 experiment and (b) composite radar image during J134 12:00 12:30

3200 m at the 14th minute to over 6000 m at the 24th minute. Since we need a two-target situation, the interferer is simulated by superimposing the CSDM of the target between the 14th and 18th minutes elongated twice in time by repeating it twice and reversed in time with 6 dB higher intensity than the target radiation.

In order to track the random radiator, the ambiguity surface at 20-m depth is displayed based on the procedure described in Fig. 7.[14] First, the ambiguity surfaces for range versus depth are constructed for each frequency and the surfaces are incoherently summed over the ten frequency components. Second, this frequency-averaged ambiguity surface

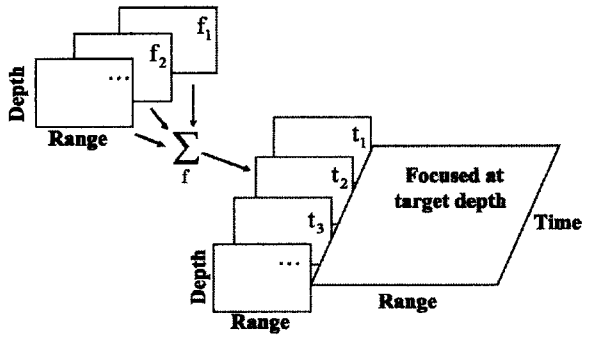

FIG. 7. Construction of ambiguity surface at fixed depth as a function of time and range.

is generated for every time step and is displayed at the selected depth where the target or interferer is located.

Figure 8(a) shows the Bartlett processor ambiguity surface at 20-m depth and Fig. 8(b) is the result from the WNC processor. The interferer trajectory superimposed with a line (running from a range of 3900 m at the 14th minute to 3200 m at the 24th minute) is clearly visible in both figures. However, the ambiguity surface from the Bartlett processor has higher sidelobes so that the trajectory of the target (running from a range of 3200 m at the 14th minute to 6000 m at the 24th minute) is barely visible. The better performance of the WNC processor than the Bartlett processor is attributed to the nulling of sources of interference as shown in Fig. 9.

The beampattern in Fig. 9(a) shows the null along the interferer track while looking at the target. Figure 9(b) shows the null with the null-broadening method using CSDM's averaged across 15 frequency bins centered on each of the frequency components. Note that the null along the trajectory of the interferer (running from a range of 3900 m at the 14th minute to 3200 m at the 24th minute) is wider as a result of the null-broadening method.

A slice of a typical nulling pattern at 62 Hz is shown in Fig. 10, which should be compared to the simulated beam pattern in Fig. 5 calculated at the same frequency. The thin line represents the nulling pattern of WNC without null-broadening and the thick line is with null-broadening where the CSDM has been averaged across 15 frequency bins.

The results at 62 Hz exhibit a somewhat fluctuating nulling pattern. Nonetheless, the frequency-averaged beam pattern in Fig. 9 shows that the null-broadening technique has been applied successfully to SWellEx-96 experimental data.

V. APPLICATION TO NULL STEERING

In this section, null-broadening in an adaptive time reversal mirror (ATRM) is discussed as an example of this technique applied to active acoustics.

The time-reversal mirror (TRM) uses the received signal from a probe source to refocus the signal at the probe source location by back-propagating the time-reversed version of the received signal. The time reversal mirror has been demonstrated in ultrasonics[15,16] and in underwater acoustics.[17] Recently, the adaptive time reversal mirror (ATRM) has been applied to steer the nulls in simulation in an ocean

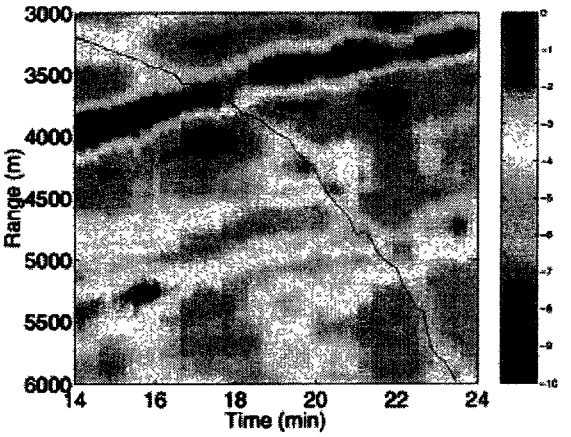

(a)

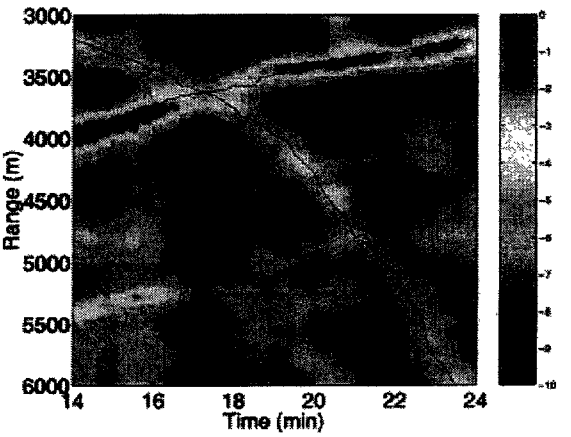

(b)

FIG. 8. Trajectories of two broadband sources at 20 m depth. (a) Power (dB) output of the Bartlett processor and (b) the WNC processor without null-broadening.

waveguide.[8] Here, we apply the null-broadening technique to the ATRM.

In Sec. V A, the theory of ATRM is reviewed and the simulation is discussed in Sec. V B.

A. Theory of the adaptive time reversal mirror

The phase-conjugate field at the field location $\vec{r}$ is written as[8]

$$p(\vec{r}) = \sum_{i=1}^{N} w_i^* g(\vec{r}|\vec{r}_i) = \mathbf{w}^\dagger \mathbf{g}(\vec{r}|\mathbf{r}_{\text{array}}), \tag{14}$$

where $\mathbf{r}_{\text{array}}$ is a column vector of array element locations and $\mathbf{g}$ is a column vector of Green's functions. The signal vector $\mathbf{w}$ reduces to $\mathbf{g}$ in a conventional time-reversal mirror.

The ATRM is accomplished by imposing two conditions on the signal vector $\mathbf{w}$ and intensity minimization:

$$\min_{\mathbf{w}} \mathbf{w}^\dagger \mathbf{K} \mathbf{w}, \tag{15}$$

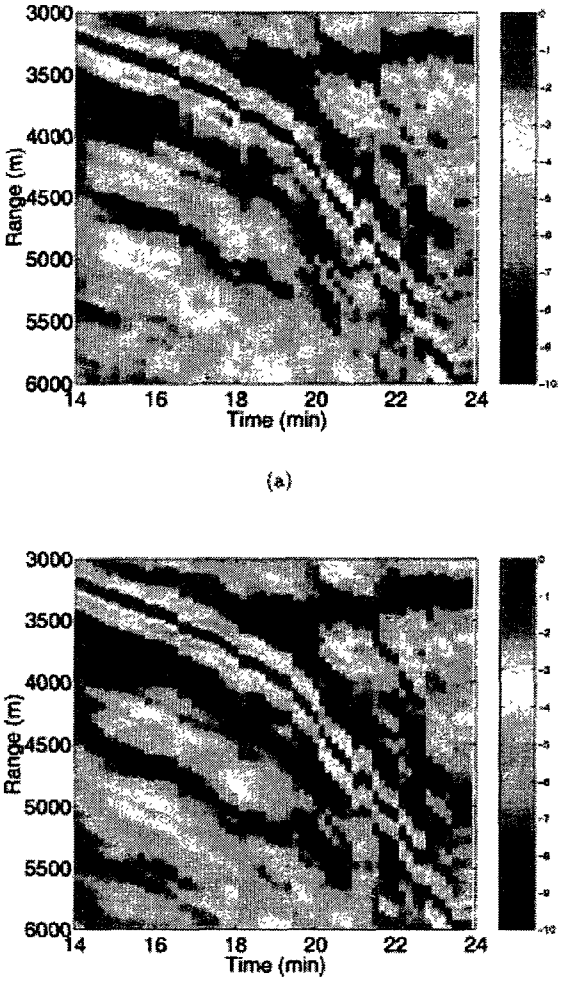

FIG. 9. Beam pattern (dB) of (a) the WNC processor without null-broadening and (b) the WNC processor with null-broadening. The beam patterns from ten frequency components are averaged incoherently to produce these plots.

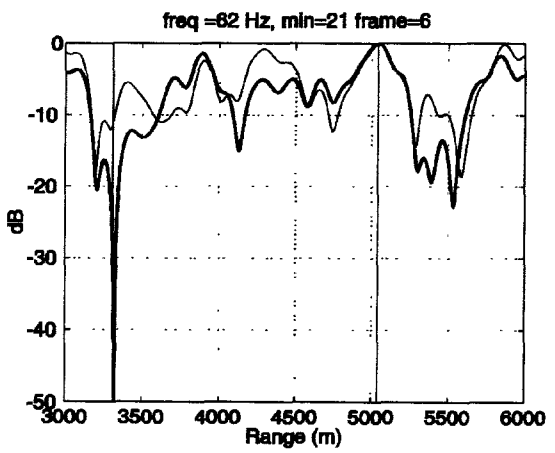

FIG. 10. Beam pattern at 62 Hz just before the 22nd minute at 20-m water depth. The beam pattern of the WNC processor without null-broadening is denoted as a thin solid line and the thick solid line is for the WNC processor with null-broadening.

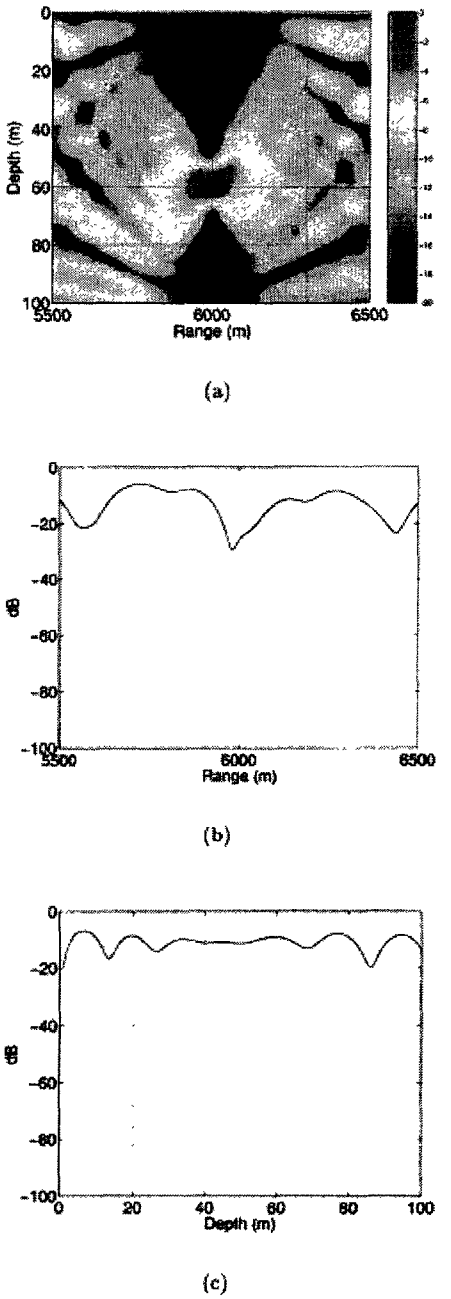

FIG. 11. (a) Contour of the focused field from the time reversal mirror. Slice of the field passing through the point B: (b) intensity versus range and (c) intensity versus depth. The intensity level is normalized so that the level at the focal point is 0 dB

and a distortionless response constraint at the focal (probe source) location which can be expressed as

$$\mathbf{w}^{\dagger}\mathbf{g}(\vec{r}_{ps}|\mathbf{r}_{\text{array}})=1. \tag{16}$$

The solution for $\mathbf{w}$ is well known and referred to as the minimum variance method in adaptive array signal processing:[10]

$$\mathbf{w}=\frac{\mathbf{K}^{-1}\mathbf{g}(\vec{r}_{ps}|\mathbf{r}_{\text{array}})}{\mathbf{g}^{\dagger}(\vec{r}_{ps}|\mathbf{r}_{\text{array}})\mathbf{K}^{-1}\mathbf{g}(\vec{r}_{ps}|\mathbf{r}_{\text{array}})}, \tag{17}$$

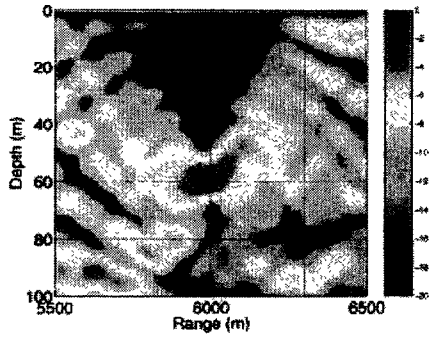

(a)

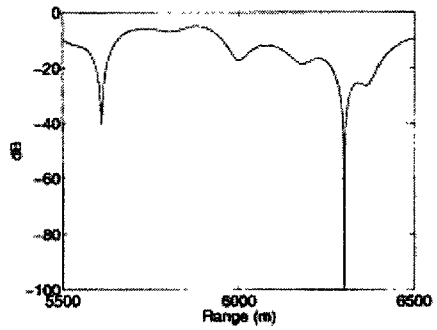

(b)

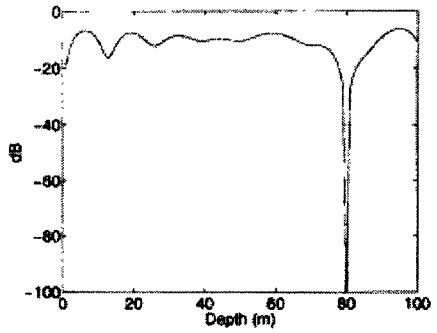

(c)

FIG. 12. (a) Contour of the focused field from the time reversal mirror with a steered null at point B. Slice of the field passing through the point B: (b) intensity versus range and (c) intensity versus depth. The intensity level is normalized so that the level at the focal point is 0 dB.

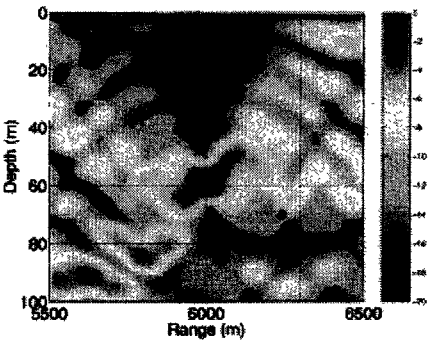

(a)

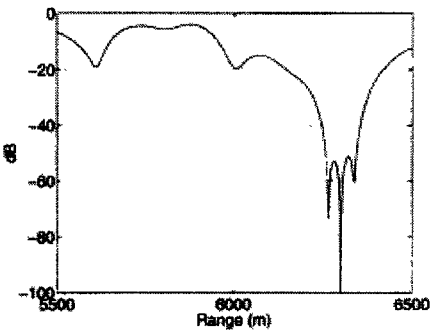

(b)

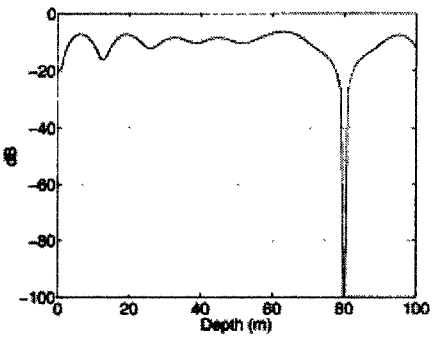

(c)

FIG. 13. (a) Contour of the focused field from the adaptive time reversal mirror with a null broadening in range at point B. Slice of the field passing through the point B: (b) intensity versus range and (c) intensity versus depth. The intensity level is normalized so that the level at the focal point is 0 dB.

where $\mathbf{K}$ is a cross spectral density matrix (CSDM).

When the CSDM is defined as[8]

$$\mathbf{K} = \mathbf{g}(\vec{r}_{p,s}|\mathbf{r}_{\text{array}})\mathbf{g}^{*}(\vec{r}_{p,s}|\mathbf{r}_{\text{array}}) + \mathbf{g}(\vec{r}_{n}|\mathbf{r}_{\text{array}})\mathbf{g}^{\dagger}(\vec{r}_{n}|\mathbf{r}_{\text{array}}), \tag{18}$$

the adaptive signal vector $\mathbf{w}$ will place a null at $\vec{r}_{n}$ since the intensity minimization requirement tends to cancel out contributions to the power except at the probe source location. In practice, the signal vector $\mathbf{w}$ is found from the minimum variance formulation with diagonal loading [e.g., the white noise constraint (WNC) in order to make it robust]. If the placement of nulls is needed at more than one location, additional outer products that correspond to the desired null locations can be added to Eq. (18).

B. Simulation

In this simulation, the same Pekeris waveguide is used as in Sec. III B and in Ref. 8. The Pekeris waveguide is 100 m deep, and the sound speed in the water column is 1500 m/s. The bottom density and sound speed are 1.5 g/cm^3 and 1600 m/s, respectively. We used 300 Hz as the center fre-

quency with a bandwidth of 1.7578 Hz yielding about 37 m null width in range in both directions.

Focusing with the time reversal mirror in a Pekeris waveguide is shown in Fig. 11(a). The level of intensity versus range and depth through point B is shown in Figs. 11(b) and (c), respectively. When a null is steered towards point B with the ATRM, the intensity is as shown in Fig. 12(a) along with horizontal and vertical slices in Figs. 12(b) and (c), respectively. Finally, Fig. 13 illustrates null broadening in range when the null broadening technique is applied to the ATRM.

VI. SUMMARY

In this paper we have described a method to broaden the null of the beam pattern of an adaptive array for reception and transmission in an ocean waveguide based on the theory of waveguide invariants. Null-broadening is demonstrated in matched field processing both in simulation and with data collected during the SWellEx-96 experiment. As another application, the null-broadening technique is demonstrated in an active acoustics example with an adaptive time reversal mirror.

ACKNOWLEDGMENTS

This work was supported by the Office of Naval Research, Grant No. N00014-94-1-0458. The authors would like to thank James Murray (MPL) for providing the data and related information for the SWellEx-96 experiment.

[1] R. J. Mailloux, "Covariance matrix augmentation to produce adaptive array pattern troughs," Electron. Lett. **31**, 771–772 (1995).
[2] M. Zatman, "Production of adaptive array troughs by dispersion synthesis," Electron. Lett. **31**, 2141–2142 (1995).
[3] J. R. Guerci, "Theory and Application of Covariance Matrix Tapers for Robust Adaptive Beam-forming," IEEE Trans. Signal Process. **47**, 977–985 (1999).
[4] S. D. Chuprov, "Interference structure of a sound field in a layered ocean," in *Acoustics of the Ocean: Current Status* (in Russian), edited by L. M. Brekhovskikh and I. B. Andreevoi (Nauka, Moscow, 1982), pp. 71–91.
[5] G. A. Grachev, "Theory of acoustic field invariants in layered waveguide," Acoust. Phys. **39**, 33–35 (1993).
[6] H. C. Song, W. A. Kuperman, and W. S. Hodgkiss, "A time-reversal mirror with variable range focusing," J. Acoust. Soc. Am. **103**, 3234–3240 (1998).
[7] G. L. D'Spain and W. A. Kuperman, "Application of waveguide invariants to analysis of spectrograms from shallow water environments that vary in range and azimuth," J. Acoust. Soc. Am. **106**, 2454–2468 (1999).
[8] J. S. Kim, H. C. Song, and W. A. Kuperman, "Adaptive time reversal mirror," J. Acoust. Soc. Am. **109**, 1817–1825 (2001).
[9] A. B. Baggeroer and H. Cox, "Passive Sonar Limits Upon Nulling Multiple Moving Ships with Large Aperture Arrays," in *Proceedings of the 33rd Asilomar Conference on Signals, Systems, and Computers*, IEEE Computer Society (1999), pp. 103–108.
[10] D. H. Johnson and D. E. Dudgeon, *Array Signal Processing—Concepts and Techniques*, Prentice Hall Signal Processing Series, Alan V. Oppenheim, Series Editor (Prentice Hall, Englewood Cliffs, NJ, 1993).
[11] H. Cox, "Robust adaptive beamforming," IEEE Trans. Acoust., Speech, Signal Process. **ASSP-35**, 1365–1376 (1987).
[12] J. Capon, "High resolution frequency wavenumber spectrum analysis," Proc. IEEE **57**, 1408–1418 (1969).
[13] N. O. Booth, A. T. Abawi, P. W. Schey, and W. S. Hodgkiss, "Detectability of low-level broad-band signals using adaptive matched-field processing with vertical aperture arrays," IEEE J. Ocean. Eng. **25**, 296–313 (2000).
[14] N. Booth, P. Schey, and W. S. Hodgkiss, "Detection of low-level broadband signals using adaptive matched-field processing," J. Acoust. Soc. Am. **101**, 3047 (1997).
[15] M. Fink, "Time-reversal mirrors," J. Phys. D **26**, 1330–1350 (1993).
[16] M. Fink, "Time-reversed acoustics," Phys. Today **50**, 34–40 (1997).
[17] W. A. Kuperman, W. S. Hodgkiss, H. C. Song, T. Akal, C. Ferla, and D. R. Jackson, "Phase conjugation in the ocean: Experimental demonstration of an acoustic time reversal mirror," J. Acoust. Soc. Am. **103**, 25–40 (1998).